Clinical & Experimental Metastasis **19:** 359–368, 2002.

Establishment of fluorescent lung carcinoma metastasis model and its real-time microscopic detection in SCID mice

Ming-Shyan Huang[1], Tzu-Jou Wang[2], Chung-Ling Liang[3], Huey-Mei Huang[1], I-Chi Yang[4], Yi-Hua Jan[4] & Michael Hsiao[4]

[1]*Department of Internal Medicine, Kaohsiung Medical University, Kaohsiung, Taiwan;* [2]*Department of Pediatrics, Kaohsiung Chang-Gung Memorial Hospital, Kaohsiung, Taiwan;* [3]*Department of Ophthalmology, Taipei Chang-Gung Memorial Hospital, Taipei, Taiwan;* [4]*Department of Medical Education and Research, Kaohsiung Veterans General Hospital, Kaohsiung, Taiwan*

Received 23 October 2001; accepted in revised form 7 January 2002

Key words: lung carcinoma, GFP, metastasis, SCID mice

Abstract

Lung cancer is the most prevalent malignant tumor in the world. Metastasis of the disease causes death in lung cancer patients. Recent study has shown that multiple cascades of gene defects occur in lung cancer. In this report, we established a novel H1299/EGFP tumor model to determine whether H1299 transfected with the enhanced green fluorescent protein (EGFP) gene *in vitro* and xenotransplanted into SCID mouse lung would permit the detection of lung cancer micrometastasis *in vivo*. We demonstrated that EGFP-transduced H1299 cells maintained stable high-level EGFP expressions during their growth *in vivo*. EGFP fluorescence clearly demarcated the primary seeding place and readily allowed for the visualization of distant micrometastasis and local invasion at the single-cell level. Small metastatic and locally invasive foci, including those immediately adjacent to the tumor's leading invasive edge, were almost undetectable by routine hematoxylin and eosin staining and immunohistochemistry. The GFP tagged lung cancer model is superior for the detection and study of physiologically relevant patterns of lung cancer invasion and metastasis *in vivo*.

Introduction

Lung cancer is the leading cause of cancer death in the world with metastasis being the major cause [1–3]. The short-term survival rate is low since most of the patients are at an advanced stage of the disease at diagnosis [4]. The skeleton, brain, liver and kidney are the most common sites for lung cancer metastasis. However, the biology of metastasis in these organs is poorly understood due to lack of a good animal model.

Revealing the cellular and molecular changes associated with cancer as they occur in intact living animal models of human neoplastic disease holds tremendous potential for understanding disease mechanisms. Models including subcutaneous implant models [5–6], renal capsule-implant models [7–9], pleural cavity [10] and orthotopic-implant models [11–14] have been established for human lung cancer. However, these models are not sufficiently representative of the clinical situation, and the early stages of tumor progression and micro-metastasis formation have been difficult to analyze because of the inability to identify small numbers of tumor cells against a background of host tissue.

Correspondence to: Michael Hsiao, Department of Medical Education and Research, Kaohsiung Veterans General Hospital, 386 Ta-Chung 1st Rd, Kaohsiung, 813 Taiwan. Tel: +886-7-3422121-1512; Fax: +886-7-3468056; E-mail: mhsiao@isca.vghks.gov.tw

Reporter genes such as beta-galactosidase, chloramphenicol acetyltransferase and luciferase have played major roles in understanding the molecular mechanisms of gene expression in cultured cells and in transgenic animals. Reporter genes have also been critically important in designing and characterizing delivery systems for gene transfer into somatic tissues in animals. However, measurement of these reporter genes in living animals requires invasive tissue sampling, either biopsy or death. Green fluorescent protein (GFP) has been used for repetitive, non-invasive reporter gene imaging in living cultured cells, single-cell organisms and multi-cellular organisms transparent to light [15–16]. The green-fluorescent protein is produced from the jellyfish *Aequorea victoria* GFP gene. The green fluorescent protein (GFP) has rapidly become a useful tool for the study of protein localization in living cells because it allows direct visualization of proteins in living cells without the need for harsh fixation methods, which can be plaqued by artifacts. Localization of any cloned protein can potentially be observed without the need for antibodies to that protein, simply by fusing the protein of interest to GFP.

Recently, an orthotopic transplant nude mouse model with GFP expressing cancer cells has been established [17]. GFP offers the strength of high-resolution *ex vivo* analyses following *in vivo* localization of the tumor [18–21]. The dynamic range of GFP detection allows the full dis-

ease course to be monitored since disease progression from small numbers of cells to extensive disease can be assessed. As such, therapies that target minimal disease as well as those designed for late stage disease can be readily evaluated in animal models. Real-time spatiotemporal analysis of tumor cell growth can reveal the dynamics of neoplastic disease, and facilitate rapid optimization of effective treatment regimens.

In this investigation, we established an orthotopic green fluorescent H1299 lung cancer model with metastatic potential in SCID mice. We also determined tumor cells' distant metastasis through vascular routes.

Materials and methods

GFP expression vector constructions

The pEGFP-C1 vector containing the enhanced green fluorescent protein gene was purchased from CLONTECH (Clontech, Palo Alto, California). To construct the EGFP-containing pCI-Neo vector, pEGFP-C1 was digested with EcoRI and NotI. The pCI-Neo vector was digested with EcoRI and NotI. The EGFP cDNA fragment was then unidirectionally subcloned into pCI-Neo. The resulting pCIEGFP-Neo vector was used to transfect lung cancer cell line.

Cell culture, transfection, and subcloning

The human lung adenocarcinoma cell line H1299 was obtained from ATCC. H1299 cells were cultured in DMEM (GIBCO) supplemented with 10% bovine calf serum (HyClone, Logan, Utah), 2 mM L-glutamine, 100 units/ml penicillin, 100 μg/ml streptomycin. H1299 cells were incubated in a humidified incubator at 37 °C with 5% CO_2. For transfection, the medium was removed; 70% confluent H1299 cells in 100-mm culture dishes were washed twice with HEPES buffer. Thereafter, H1299 cells were incubated with a mixture of liposome transfection reagent (10 μg DNA in 1.5 ml HEPES buffer + 100 nM DOTAP/Cholesterol liposome in 1.5 ml HEPES buffer) for 4 h before being replenished with a fresh medium. Forty-eight hours after transfection, H1299 cells were examined by fluorescence microscopy for the presence of EGFP positive cells. For selection of EGFP transductants, cells were cultured in a selective medium containing 800 μg/ml of G418 for 7 days or until the mock transfected cells died. Cells expressing the EGFP gene were maintained in selection medium containing 200 μg/ml of G418. H1299 clones expressing EGFP (H1299-EGFP) were isolated with cloning cylinders (Bel-Art Products, Pequannoch, New Jersey) by trypsin/EDTA and were transferred and amplified by conventional culture methods. A total of 12 high GFP expressing clones were selected and expanded. These clones were used to establish an *in vivo* tumor.

In vitro *and* in vivo *growth curves*

H1299 and H1299/EGFP cells were seeded at 1×10^5 in 12-well plates in triplicate. The cells were harvested and counted every day for 5 days to determine the *in vitro* growth curves. To determine the *in vivo* growth potential, H1299 and H1299/EGFP were grown without G418 for 48 h. Thereafter, 5×10^6 cells were injected into the flanks of SCID mice. Twelve injections of both H1299 and H1299/EGFP in twelve mice were performed. Tumor volume was measured every week until the mice were sacrificed. Standard deviations and statistics were calculated to generate the *in vitro* and *in vivo* growth curves.

Orthotopic injection

The method for orthotopic injection was as described (17) with some modifications. Briefly, the mice were anesthetized by KXA cocktail injection as described [22]. The animals were put in a position of right lateral decubitus, with four limbs restrained. A 0.8-cm transverse incision of skin was made in the left chest wall. Chest muscles were separated by sharp dissection, and costal and intercostal muscles were exposed. A 0.4–0.5-cm intercostal incision between the third and fourth rib on the chest wall was made, and the chest wall was opened. The left upper lobe was taken up by forceps, and 1 mm^3 of H1299/EGFP subcutaneous tumor chunk was minced and promptly injected into the upper lung by a Hamilton syringe (injection 2 min and retraction 2 min) with a 30 gauge needle. The lung was then returned into the chest cavity after confirmation that there was no tumor cell leakage through the whole process. The incision in the chest wall was closed with a 7-0 surgical suture. A 3 ml syringe with a 25 gauge needle was then used to remove pleural cavity air through intrathoracic puncture. Intrathoracic puncture was performed with a 25 gauge needle attached 3 ml syringe to remove pleural cavity air after chest wall closure. The skin and chest muscle were closed with Autoclips (MikRon Precision Inc, Gardena, California). All procedures were performed under a 7× microscope (Leica, Germany).

Analysis of EGFP tumor metastasis in real-time

After the tumor had been established in SCID mice, the performance status of the mice began to decrease. The animals were sacrificed and subjected to fluorescent microscopy examinations when clinical symptoms of terminal illness appeared. The fresh tumors and all major organs were examined for the presence of fluorescence directly under a Zeiss inverted fluorescent microscope equipped with a 100 W mercury lamp power supply, EGFP filter sets (Chroma Technology, Brattleboro, Vermont), and NIKON CoolScan 95 digital camera. Images were captured at the resolution of 1,600 × 1,200 pixels and transferred directly to a PC computer for analysis.

Histopathological analyasis

Primary tumors and all organs from different injection routes were subjected to histopathological analysis. Tumors and

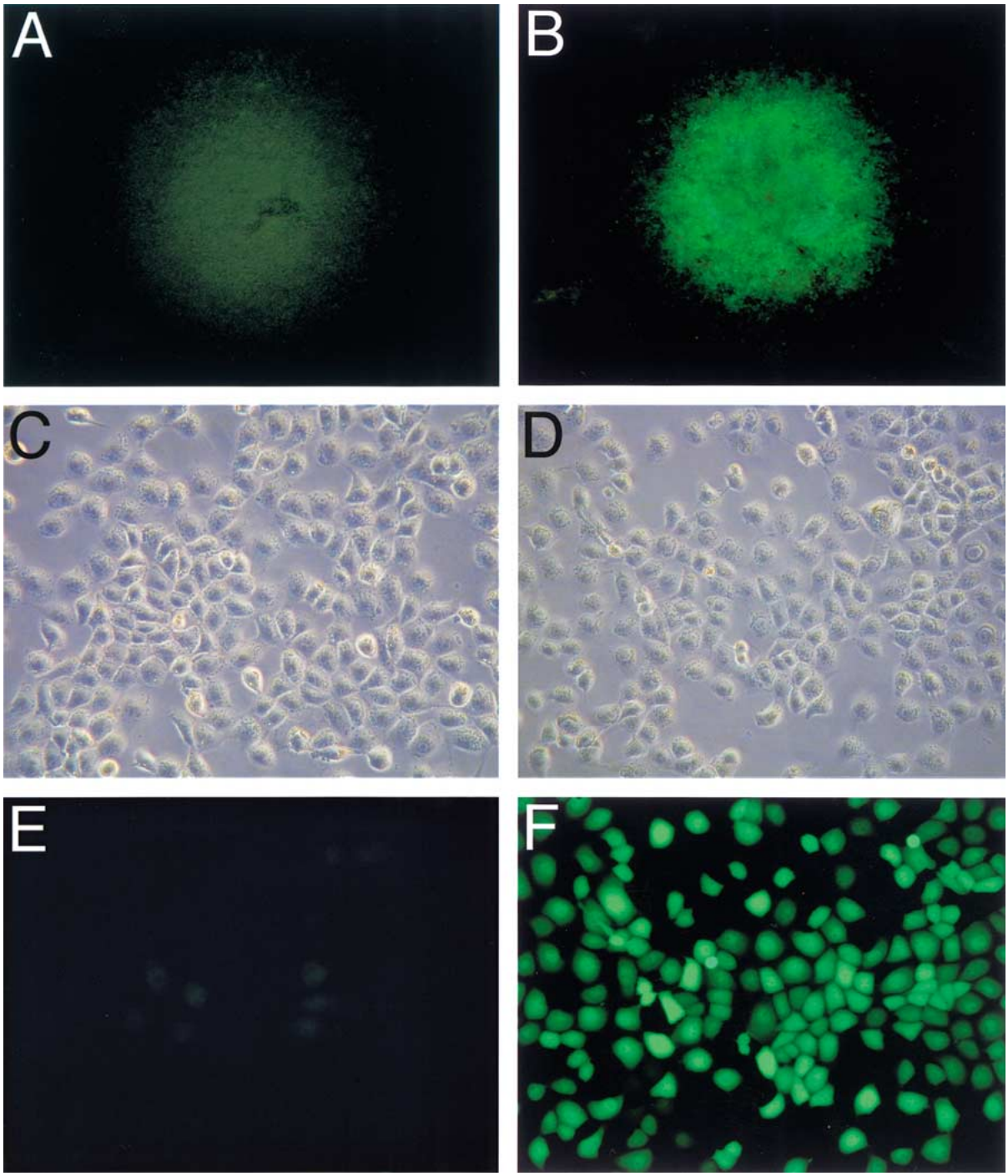

Figure 1. Stable and high-level GFP expressions in H1299 cells. Human non-small-cell lung cancer cell line H1299 was transfected with pCIEGFP-Neo expression vector, which expresses EGFP and the neomycin resistance genes. Stable, high-expression clones were selected in 800 μg/ml G418. (A) Vector control, no green fluorescence was detected (40×). (B) Strong green fluorescence was detected in H1299/EGFP transductants *in vitro* (40×). (C–D) Daylight pictures of cells from Vector control (C, 400×) and H1299/EGFP (D, 400×). Note H1299/EGFP showed similar parental H1299 morphology. (E–F) H1299 and H1299/EGFP pictures under fluorescent microscope. Note strong cytoplasmic green fluorescence detected in 100% of H1299/EGFP cell (F, 400×) compared to control (E, 400×).

tissues were fixed in 3.7% formaldehyde, 5% glacial acetic acid, and 72% ethanol for at least one day before proceeding to paraffin embedding. Serial 4 μm sections were cut and stained with hematoxylin and eosin for histopathological examinations.

Results

Isolation of stable and high-level GFP expression H1299 cells

EGFP- and neomycin-transduced H1299 cells were selected for resistant cells at 800 μg/ml of G418. Several high GFP expressing cell clones were selected. These selected

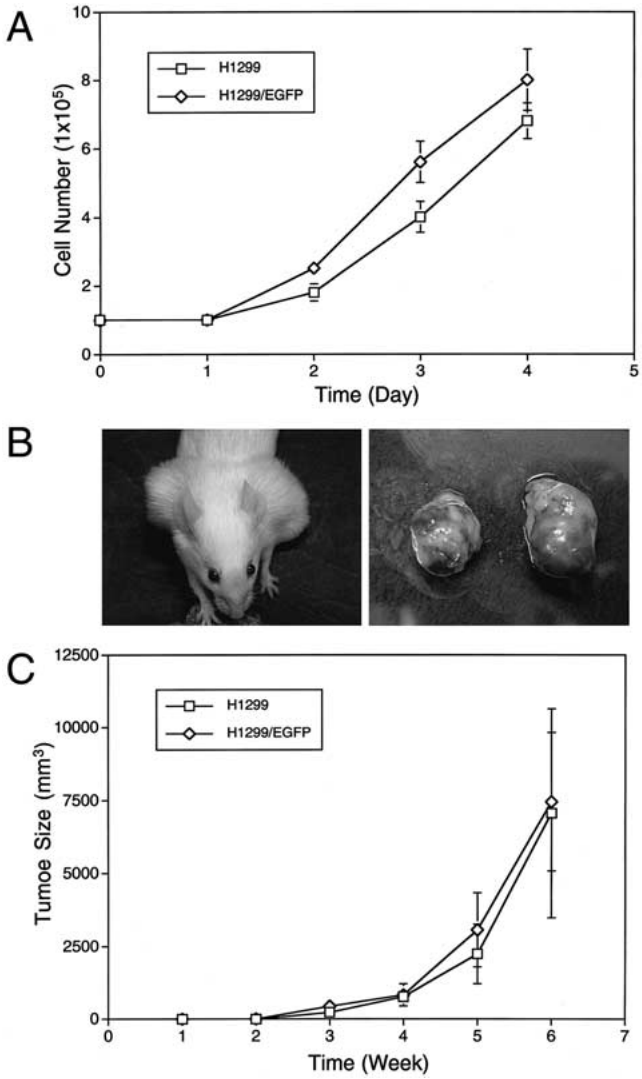

Figure 2. *In vitro* and *in vivo* tumor growth curves of human H1299/EGFP cells. (A) *In vitro* growth curves of H1299/VC and H1299/EGFP cells. No statistical difference between H1299/VC and H1299/EGFP was observed. (B) Frontal view of subcutaneous tumors 5 weeks after subcutaneous implantation of H1299 and H1299/EGFP cells. Left: H1299 cells only. Right: tumor developed from H1299/EGFP cells implantation. (C) *In vivo* growth curves of H1299 and H1299/EGFP tumors. No difference in tumor size was observed between the H1299 and H1299/EGFP induced tumors.

H1299/EGFP cells had strikingly bright EGFP fluorescence that remained stable in the absence of selective agents after more than 20 passages (Figures 1B, F) compared to vector control (Figures 1A, E). There was no difference in the doubling-time of parental cells and selected transduced cells as determined by comparison of proliferation in monolayer culture (Figure 2A). More than five high GFP expressing H1299 clones were pooled and injected into SCID mice to establish *in vivo* tumors.

Stable and high-level GFP expression of H1299/EGFP tumors in SCID mice

Mice receiving a subcutaneous injection of H1299/EGFP cells were sacrificed after six weeks. All of the mice had subcutaneous tumors, ranging from 3,000 mm^3 to 11,500 mm^3 (mean 7,500 mm^3, Figures 2B and C). No statistical difference in tumor size between the H1299 and H1299/EGFP induced tumors was observed (Figure 2C). These results showed that the existence of green fluorescent protein in H1299 tumor cells did not interfere with the tumorigenicity or tumor growth.

Histopathological and fluorescent imaging analyses of H1299/EGFP subcutaneous tumors

Figure 3 shows serial sections of paraformaldehyde fixed subcutaneous tumors. Histopathological and fluorescent microscopy findings of the excised subcutaneous tumors showed local invasions of H1299/EGFP into adjacent muscle layers (Figures 3B and E), suggesting the malignant nature of H1299/EGFP tumor cells.

External fluorescence image analysis of H1299/EGFP orthotopic tumors established in lung

In the left lung of 20 SCID mice, 1 mm^3 H1299/EGFP tumor tissues derived from the H1299/EGFP subcutaneous tumors were implanted by intrapulmonary injections. All the necrotic areas in the subcutaneous tumors (near the center of the s.c. tumor) were excluded for implantation to avoid the interference in growth and metastasis potential caused by necrotic debris. Multiple live tumor foci were found two weeks after implantation. These tumor foci in excised lung were visualized directly under an inverted fluorescent microscope to identify the presence of H1299/EGFP cells (Figures 4A–C). Micrometastasis into deep lung parenchyma was also noted (Figures 4D, E). Contralateral metastasis into the right lung was found three weeks after implantation (Figure 4F).

Real-time fluorescence image analysis of H1299/EGFP metastases in multiple organs

Six weeks after orthotopic implantation of H1299/EGFP tumor fragments (1 mm^3), metastatic foci were found in multiple organs including kidney, colon, liver, brain, heart, and spleen (Table 1). External images of organs revealing the presence of live H1299/EGFP tumor cells under an inverted fluorescent microscope are shown in Figure 5. Newly established H1299/EGFP tumor metastasis foci were found mainly in kidney (Figures 5A–B) and colon (Figures 5C–D) four weeks after implantation. The renal parenchyma was demonstrated by the presence of convoluted tubules in the background, as shown in Figure 5B. Figures 5E–H demonstrate that micrometastasis at a single-cell level could be detected in liver and brain. These results showed the preference of H1299/EGFP tumor cells to metastasize to these organs after orthotopic implantation into lung parenchyma. Other organs or tissues such as ovary, bone marrow, bladder, pancreas, lymph nodes and muscles did not reveal the presence of H1299/EGFP cells at six weeks after implantation.

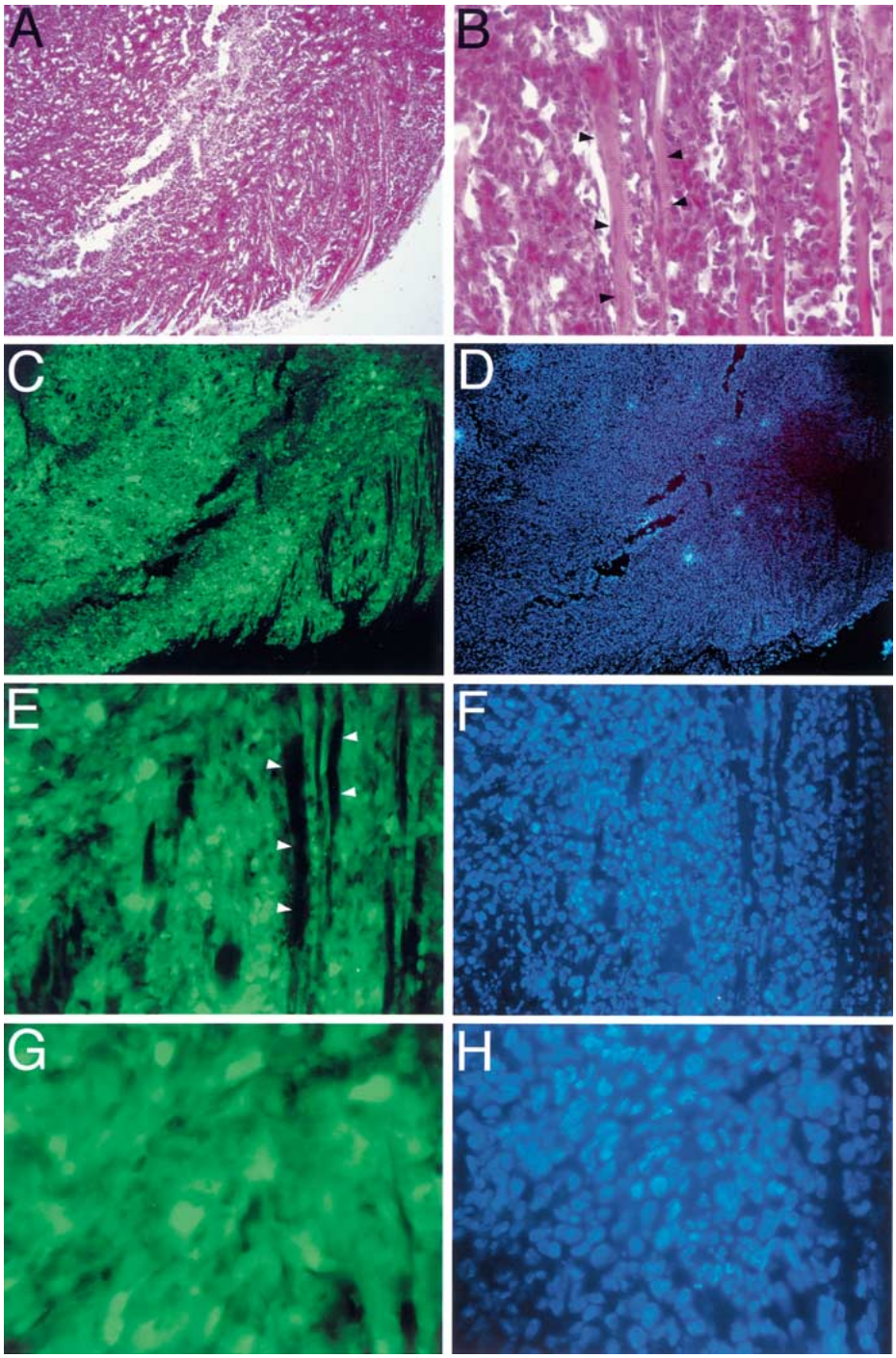

Figure 3. Histopathology of the H1299/EGFP induced subcutaneous tumor. (A–B) Histopathology of paraformaldehyde fixed H1299/EGFP subcutaneous tumors (H&E stain, A, 40×, B, 200×). (C, E, G) fixed H1299/EGFP tumors showed extensive and strong green fluorescence in every tumor cell (C, 40×; E, 200×; G, 400×). (D, F, H) Hoechst counterstain of the nucleus in fixed tumor sections correlating to C, E, G (D, 40×; F, 200×; H, 400×). Arrow heads show tumor invasion into muscle layers (B, pink muscle fibers observed under daylight; E, dark images observed under FITC channel). Also note that tumor cells were of normal and healthy morphology with round and large nucleus in H1299/EGFP tumors (F and H).

Visualizations of EGFP-expressing tumor micrometastasis through vascular routes

Fluorescent real-time images were captured to determine the route of the H1299/EGFP tumor metastases. Peripheral vasculatures and lymphatic ducts were observed in various live organs. Figure 6 showed H1299/EGFP cells in colon (Figures 6A–B), brain (Figures 6C–D) and liver blood vessels (Figures 6E–F). The free flowing tumor cells inside the brain peripheral vessels remained round and became flattened when attached to the vessel wall (Figure 6D). The arrowhead in Figure 6D demonstrates a tumor cell penetrating the vessel wall. The micrometasis of H1299/EGFP tumor cells through the vascular route was further evidenced by tumor cells flowing out of the manually cut blood vessels, as shown in Figures 5A–B.

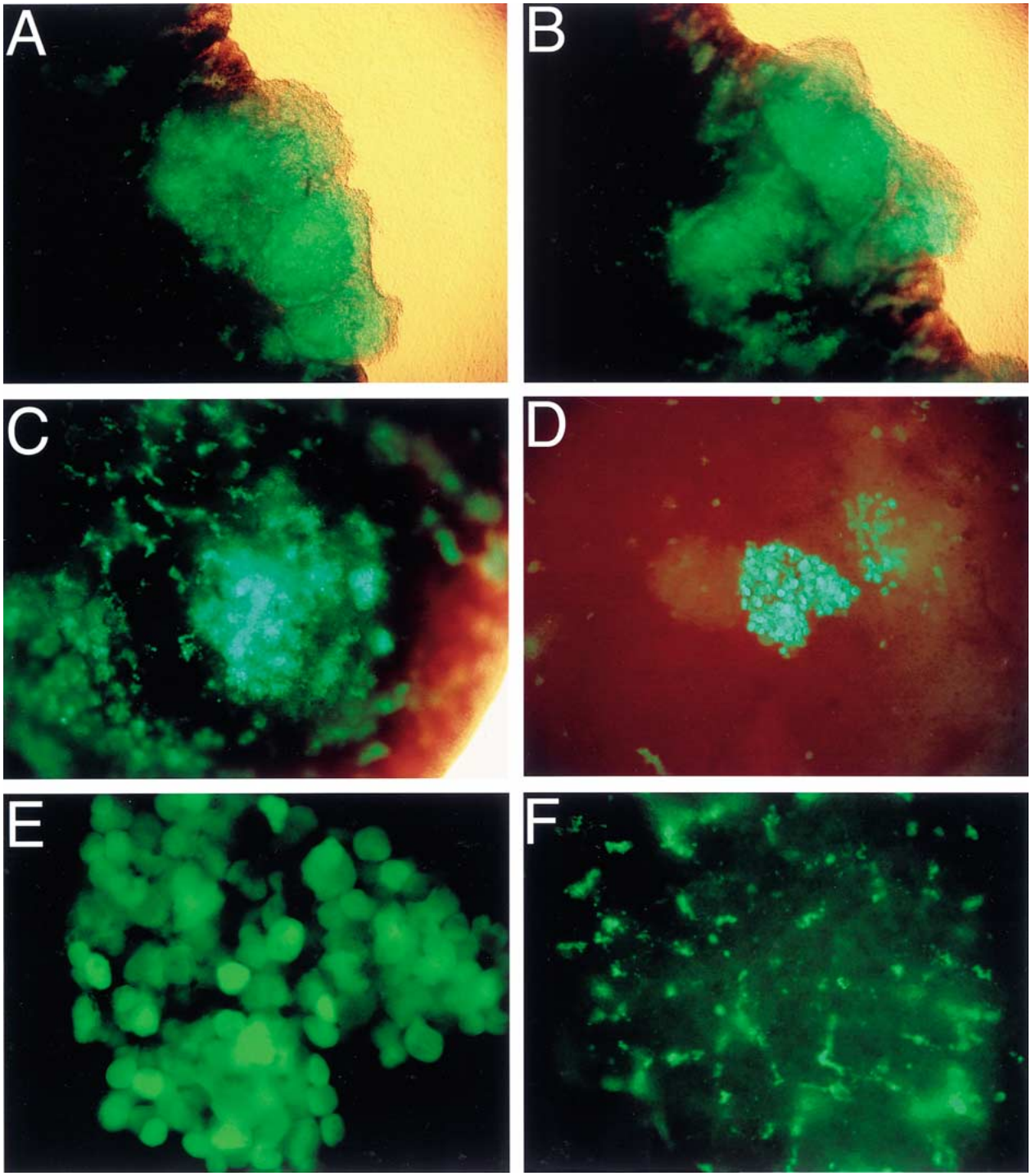

Figure 4. External images of live H1299/EGFP orthotopic lung tumors. (A–C) Live H1299/EGFP tumor foci in lung were excised from the animal and imaged in real-time by inverted fluorescence microscope. (D–E) Clear images of one tumor focus in deep lung parenchyma (B, 40×; D, 400×). (F) Contralateral tumor micrometasis in the right lung were imaged two weeks after orthotopic injection.

Discussion

The present study intended to establish a human non-small-cell lung carcinoma metastasis model in mice and showed that brain, liver, colon, and kidney are the most commonly involved sites of human H1299-EGFP lung tumor metastases. Previously, Rashidi et al. established orthotopic GFP Lewis lung carcinoma model in nude mice [23] and showed metastases on the ipsilateral diaphragmatic surface, contralateral lung parenchyma, and in mediastinal lymph nodes. In addition, heart metastases were visualized in 40%, and brain metastases were visualized in 30% of the SOI animals. However, Lewis lung carcinoma, derived from a spontaneous epidermoid carcinoma of the lung in mouse, may not represent true human non-small-cell lung carcinoma. Our results were also different from a previous study by Yang et al., as no systemic organ metastasis except the skeleton and contralateral lung metastasis were found [17]. This may

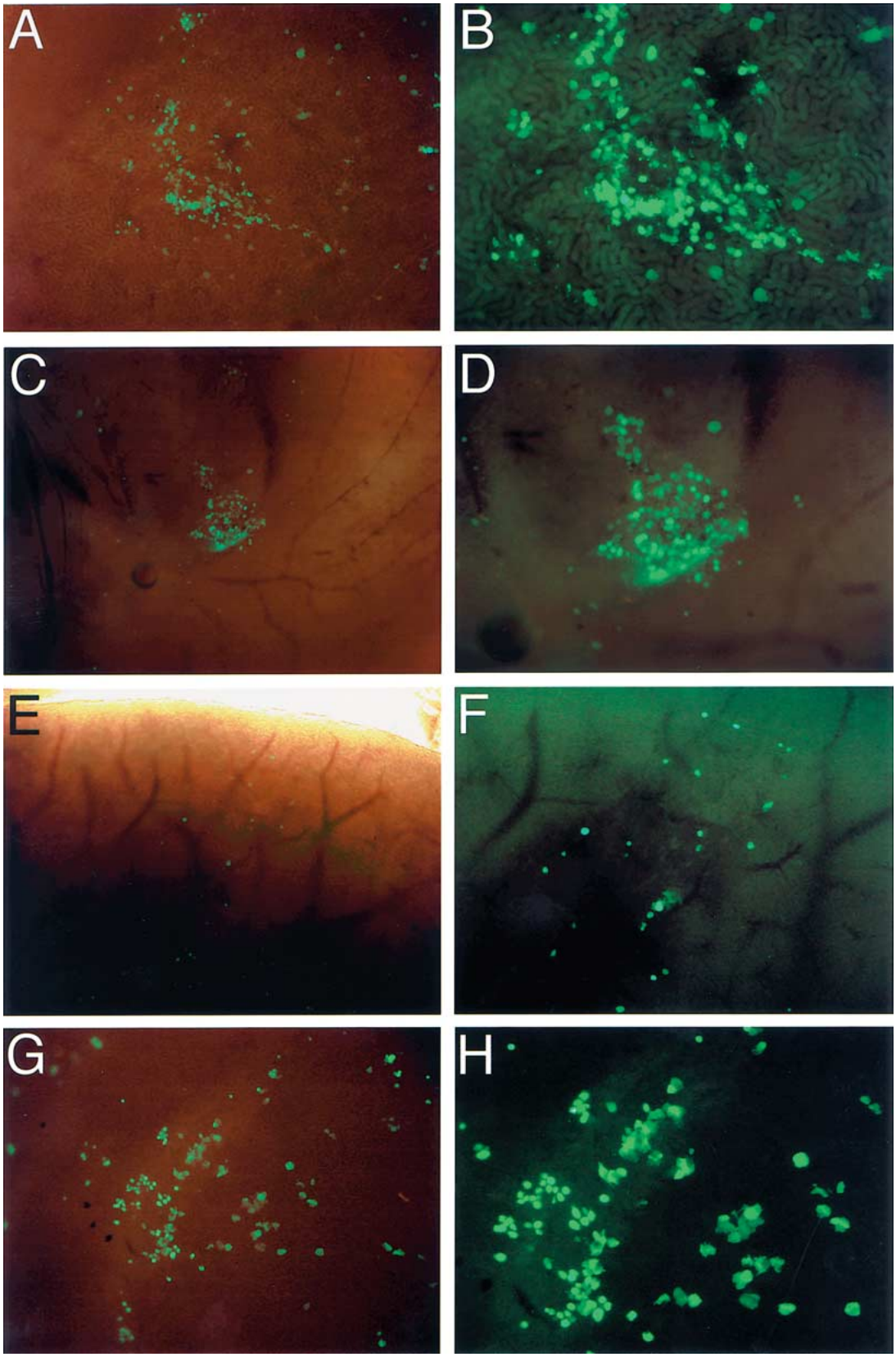

Figure 5. External images of live H1299/EGFP metastatic tumors in multiple organs. (A–B) GFP image of kidney showed multiple metastatic foci (A, 40×; B, 200×). The background in B showed convoluted tubules indicative of renal parencymal. (C–D) GFP image of colon showed metastatic lesions. (C, 40×; D, 200×). (E–F) GFP image of liver; the GFP can be detected at single-cell level (E, 40×; F, 200×). (G–H) GFP image of the metastatic tumor in the brain (G, 40×; H, 200×).

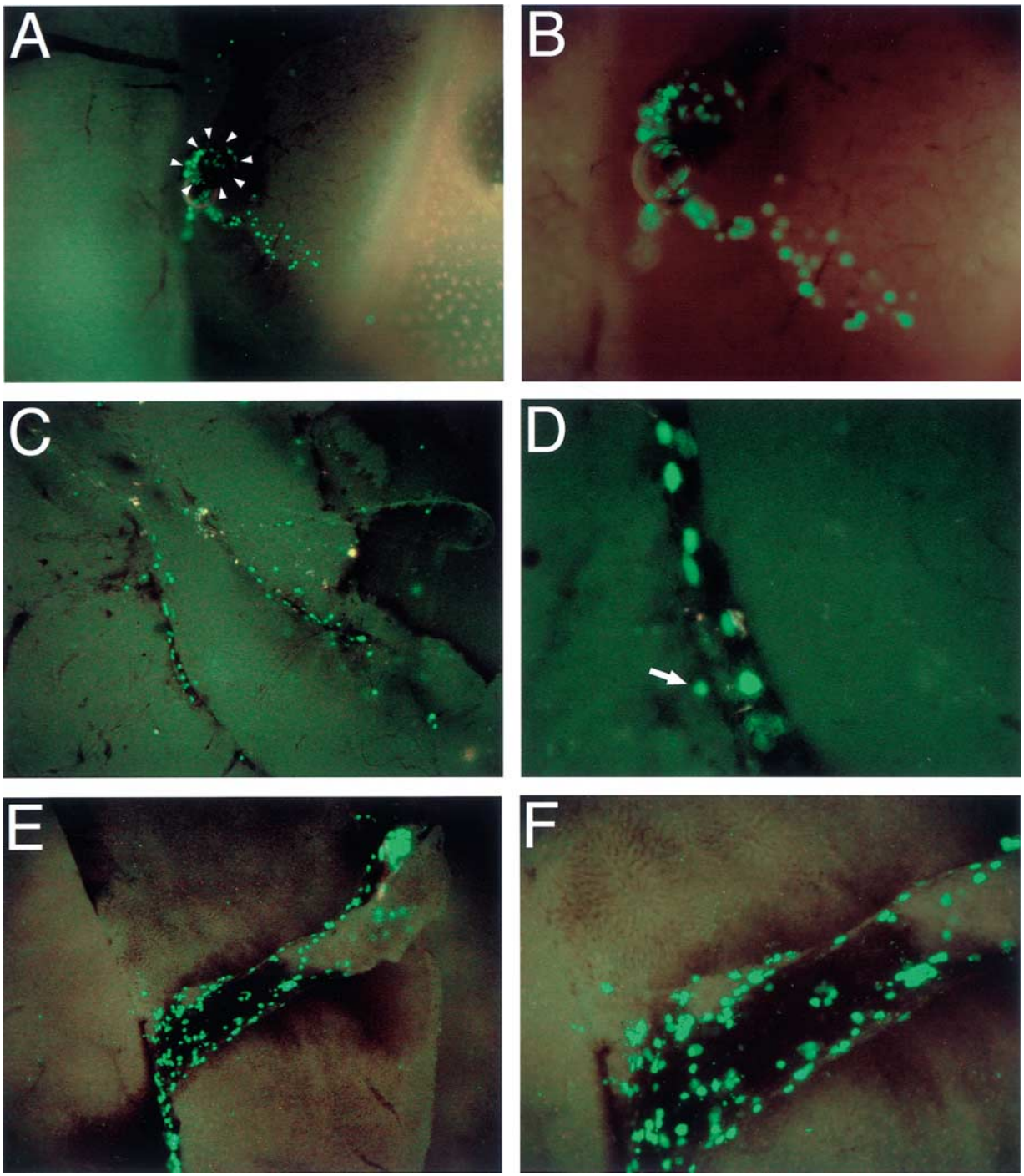

Figure 6. Real-time visualization of live H1299/EGFP tumor micrometastases through vascular routes. (A–B) The fluorescent H1299/EGFP tumor cells flowed out from manually cut blood vessels in live tissue. Arrow heads indicate the diameter of the blood vessel (A, 40×; B, 200×). (C) The H1299/EGFP tumor cells were found in the blood vessel of the live brain (40×). (D) Same area as in C under high power field; the H1299/EGFP cells became flattened when attached to the vessel wall. Free flowing tumor cells remained round in the vascular lumen. (E–F) H1299/EGFP cells were also detected in live liver sinusoids (E, 40×; F, 200×).

be due to the different mouse strain used, since a nude mouse model was used in their system. Models based on athymic nude mice have normally been used for human cancer research. Many human epithelial and hematopoietic tumors that do not grow in nude mice can grow in SCID mice [24, 25] and induce diseases more similar to what is observed in humans [26]. In addition, lung cancers established in SCID mice were found to be superior to nude mice in higher metastasis frequency and shorter metastasis period [27, 28]. The resistant immune surveillance factors were less prominent in SCID compared to nude mice [29]. In addition, the microenvironment may also influence the growth of tumor cells [30, 31]. This may explain in part the different results observed between our studies.

Metastasis in H1299 lung cancer is believed to be the result of direct tumor invasion (Figures 3 and 4) or brought

Table 1. Metastasis of GFP-expressing H1299 cells after orthotopic implantation in SCID mice.

	Tumor spread										
Mouse#	Lung	Pleural membrane	Liver	Spleen	Kidney	Heart	Intestine	Brain	Ovary	Peritoneum	Bone marrow
1	+	+	+	+	+	+	+	+		+	
2	+	+	+	+	+	+	+			+	
3	+	+	+	+	+	+		+			
4	+	+	+	+	+	+		+			
5	+	+	+	+	+	+	+	+		+	
6	+	+	+	+	+	+					
7	+	+	+	+	+	+		+			
8	+	+	+		+	+		+			
9	+	+	+	+	+	+	+	+		+	
10	+	+	+	+	+	+	+	+		+	

1 mm^3 of H1299-GFP subcutaneous tumor in SCID mice was harvested and minced. The resulting fragments were then re-injected into SCID mouse lung. Six weeks after implantation, the animals were sacrificed and the fresh tissues were explored for tumor spread by GFP expression using a fluorescent microscope.

about through the vascular route with extravascular invasion (Figure 6). The use of H1299/EGFP cells in this study enables us to visualize the extensive metastatic processes by observing the migrations of EGFP protein expressed H1299 cells in SCID mice directly under a fluorescence microscope. This method can distinguish metastatic tumor cells from normal tissue with a higher resolution.

X-rays, MRI, and ultrasonography have all been used to perform external imaging of internally growing tumors. Although these methods are well suited to the noninvasive imaging of large-scale structures in the human body [32], they have limitations as regards the investigation of internal growing tumors. This conventional optical imaging has been severely limited by the strong absorbance and scattering of the illuminating light by tissue surrounding the target, resulting in insufficient sensitivity and spatial resolution to image early-stage tumor growth or metastasis [33]. In addition, monitoring growth and metastatic dissemination by these methods is impractical because they either use potentially harmful irradiation or require harsh contrast agents and, therefore, cannot be repeated on a frequent, real-time basis. Other attempts, such as using labeled monoclonal antibody and other high-affinity vector molecules targeted against tumor-associated markers as specific, detectable spatial markers, have met mostly with indifferent success [34–38]. The luciferase gene, which emits light, has also been developed to monitor spatial temporal gene expression in animals [39, 40]. However, transferring of luciferase substrate into mammalian cells is required. Also, time duration of the luciferase gene expressions in metastatic tumors was not determined. Weissleder et al. described a novel approach to image live tumors [41]. This approach required infusion of protease-activated, near infra-red fluorescent probes to make the target tissue selectively fluorescent. Tumors with appropriate proteases could activate the probes and be imaged externally. However, most normal tissues also have significant protease activity in addition to short half-life of the fluorescence probes that may hamper the detection of tumors.

In this study, we used EGFP gene insertions into a lung cancer cell line to produce tumors that could be viewed real-time by means of fluorescence. Stable green fluorescent protein (GFP) expression in cancer cells has previously been shown to be an effective tumor cell marker compared to conventional pathological examination procedures such as histology and immnunohistochemistry. Single-cell level detection sensitivity can be achieved to visualize tumor motility, progression, and metastasis [42–44]. The imaging of the GFP-expressing tumor cells requires no preparative procedures and is well suited to visualizing live tissue. In conclusion, we have used EGFP inserted H1299 lung cancer cells to establish a novel metastasis lung cancer model in SCID mice. We showed extensive distributions of tumor micrometastasis even at single-cell level in major organs such as liver, brain, kidney, and colon. The invasion and extravasation processes can be monitored in real-time. The SCID mouse model may be a better animal model for human metastatic lung cancer compared to a nude mouse model.

Acknowledgements

We thank Ms Yu-Jung T. Liao and Mr Jing-Dung Chou for help in animal surgery. This study was supported by grants from the National Science Council (90-2314-B-037-070 to M.S.H., 90-2314-B-182A-027 to T.W., and 90-NU-7-075B-001 to M.H.), Chang-Gung Memorial Hospital (CMRP1248 to T.W.), and Kaohsiung Veterans General Hospital (VGHKS90-08 and VGHKS91-19 to M.H.).

References

1. Silverberg E. Cancer statistics. CA Cancer J Clin 1985; 35: 19–35.
2. Horn JW, Asire AJ, Young JL et al. SEER program: Cancer incidence and mortality in the United States, 1973–1981. Bethesda, Maryland: Department of Health and Human Services, NIH Publication 1984; 85–1837.
3. Loeb LA, Ernster VL, Warner KE et al. Smoking and lung cancer: An overview. Cancer Res 1984; 44: 5940–58.

4. Arguello F, Baggs RB, Rantz CN. A murine model of experimental metastasis to bone and bone marrow. Cancer Res 1988; 48: 6876–81.
5. Fidler IJ. Rationale and methods for the use of nude mice to study the biology and therapy of human cancer metastasis. Cancer Metastasis Rev 1986; 5: 29–49.
6. Sharky FE, Fogh J. Consideration in the use of nude mice for cancer research. Cancer Metastasis Rev 1984; 3: 341–60.
7. Aamadal S, Fodstad O, Pihl A. Human tumor xenografts transplanted under the renal capsule of conventional mice. Growth rate and host immune response. Int J Cancer 1984; 34: 725–30.
8. Aamadal S, Fodstat O, Pihl A. Methodological aspects of the 6-day subrenal capsule assay for measuring response of human tumors to anticancer agents. Anticancer Res 1985; 5: 329–38.
9. Bogden AE, Haskell PM, Lepage DJ et al. Growth of human xenografts implanted under the renal capsule of immunocompetent mice. Exp Cell Biol 1996; 47: 281–93.
10. Nagamachi Y, Tani M, Shimizu K et al. Orthotopic growth and metastasis of human non-small cell lung carcinoma cell injected into the pleural cavity of nude mice. Cancer Lett 1998; 127: 203–9.
11. McLemore TL, Eggleston JC, Shoemaker RH et al. Comparison of intrapulmonary, percutaneous intrathoracic, and subcutaneous models for the propagation of human pulmonary and nonpulmonary cancer cell lines in Athymic mice. Cancer Res 1998; 48: 2880–6.
12. MeLemore TL, Liu MC, Blacker PC et al. Novel intrapulmonary model for othotopic propagation of human lung cancers in athymic nude mice. Cancer Res 1987; 47: 5132–40.
13. Wang X, Fu X, Hoffman RM. A new patient-like metatstatic modle of human lung cancer onstructed orthotopically with intact tissue via throacotomy in immunodeficient mice. Int J Cancer 1992; 51: 992–5.
14. Wang X, Fu X, Hoffman RM A patient-like metastasizing model of human lung adnocarcinoma constructed via thoractomy in nude mice. Anticancer Res 1992; 12: 1399–402.
15. Chalfie M, Tu Y, Euskirchen G et al. Green fluorescent protein as a marker for gene expression. Science 1994; 263: 802–5.
16. Chalfie M. Green fluorescent protein. Photochem Photobiol 1995; 62: 651–6.
17. Yang M, Hasegawa S, Jiang P et al. Widespread skeletal metastatic potential of human lung cancer revealed by green fluorescent protein expression. Cancer Res 1998; 58: 4217–21.
18. Yang M, Baranov E, Jiang P et al. Whole-body optical imaging green fluorescent protein-expressing tumors and metastasis. Proc Natl Acad Sci USA 2000; 97: 1206–11.
19. Yang M, Baranov E, Moosa AR et al. Visualizing gene expression by whole-body fluorescence imaging. Proc Natl Acad Sci USA 2000; 97: 12278–82.
20. Yang M, Baranov E, Li XM et al. Whole-body and intravital optical imaging of angiogenesis in orthotopically implanted tumors. Proc Natl Acad Sci USA 2001; 98: 2616–21.
21. Contag CH, Jenkins D, Contag PR. Use of reporter genes for optical measurements of neoplastic disease *in vivo*. Neoplasia 2000; 2: 41–52.
22. Hsiao M, Tse V, Carmel J et al. Functional expression of human p21WAF1/CIP1 gene in rat glioma cells suppresses tumor growth *in vivo* and induces radiosensitivity. Biochem Biophys Res Comm 1997; 233: 329–35.
23. Rashidi B, Yang M, Jiang P et al. A highly metastatic Lewis lung carcinoma orthotopic green fluorescent protein model. Clin Exp Metastasis 2000; 18: 57–60.
24. Philips RA, Jewett MAS, Gallie BL. Growth of human tumors in immune-deficient SCID mice and nude mice. Curr Top Microbiol Immunol 1989; 152: 259–63.
25. Xie X, Brunner N, Jensen G et al. Comparative studies between nude and SCID mice on the growth and metastatic behavior of xenografted human tumors. Clin. Exp Metastasis 1992; 10: 201–10.
26. Huang YW, Richardson JA, Tong AW et al. Disseminated growth of a human multiple myeloma cell line in mice with severe combined immunodifiency disease. Cancer Res 1993; 53: 1392–6.
27. Wang X, Fu X, Hoffman RM. A new patient-like metastatic model of human lung cancer constructed orthotopically with intact tissue via thoractomy in immunodeficiency mice. Int J Cancer 1992; 51: 992–5.
28. Mueller BM, Romerdahl CA, Trent JM et al. Suppression of spontaneous melanoma metastasis in SCID mice with an antibody to the epidermal growth factor receptor. Cancer Res 1991; 51: 2193–8.
29. Yano S, Nishioka Y, Izumi K et al. Novel metastasis model of human lung cancer in SCID mice depleted of NK cells. Int J Cancer 1996; 67: 211–7.
30. Arguello F, Baggs RB, Eskenazi AE et al. Vascular anatomy and organ-specific tumor growth as critical factors in the development of metastases and their distribution among organs. Int J Cancer 1991; 48: 583–90.
31. Hara Y, Ogata Y, Shirouzu K. Early tumor growth in metatstatic organs influenced by the microenvironment is an important factor which provides organ specificity of colon cancer metastasis. J Exp Clin Cancer Res 2000; 19: 497–504.
32. Tearney GJ, Brezinski ME, Bouma BE et al. *In vivo* endoscopic optical biopsy with optical coherence tomography. Science 1997; 276: 2037–9.
33. Taubes G. Play of light opens a new window into the body. Science 1997; 276: 1991–3.
34. Baum RP, Brummendorf TH. Radioimmunolocalization of primary and metastatic breast cancer. Q J Nucl Med 1998; 42: 33–42.
35. Teates CD, Parekh JS. New radiopharmaceuticals and new applications in medicine. Curr Probl Diagn Radiol 1993; 22: 229–66.
36. Dessureault S, Koven I, Reilly RM et al. Pre-operative assessment of axillary lymph node status in patients with breast adenocarcinoma using intravenous 99mtechnetium mAb-170H.82 (Tru-Scint AD). Breast Cancer Res Treat 1997; 45: 29.
37. Pasqualini R, Koivunen E, Ruoslahti R. Alpha v integrins as receptors for tumor targeting by circulating ligands. Nat Biotechnol 1997; 15: 542–6.
38. Neri D, Carnelmolla B, Nissim A et al. Targeting by affinity-matured recombinant antibody fragments of an angiogenesis associated fibronectin isoform. Nat Biotechnol 1997; 15: 1271–5.
39. Edinger M, Sweeney TJ, Tucker AA et al. Noninvasive assessment of tumor cell proliferation in animal models. Neoplasia 1999; 1: 303–10.
40. Sweeney TJ, Mailander V, Tucker AA et al. Visualizing the kinetics of tumor-cell clearance in living animals. Proc Natl Acad Sci USA 1999; 96: 12044–9.
41. Weissleder R, Tung CH, Mahmood U et al. *In vivo* imaging of tumors with protease-activated near-infrared fluorescent probes. Nat Biotechnol 1999; 17: 375–8.
42. Farina KL, Wyckoff JB, Rivera J et al. Cell motility of tumor cells visualized in living intact primary tumors using green fluorescent protein. Cancer Res 1998; 58: 2528–32.
43. Chishima T, Miyagi Y, Wang X et al. Cancer invasion and micrometastasis visualized in live tissue by green fluorescent protein expression. Cancer Res 1997; 57: 2042–7.
44. Paris S, Chauzy C, Martin-Vandelet N et al. A model of spontaneous lung metatstasis visualized in fresh host tissue by green fluorescent protein expression. Clin Exp Metastasis 1999; 17: 817–22.